

Journal of Al-Azhar University Engineering Sector



Vol. 20, No. 77, October 2025, 1453 - 1473

NUMERICAL ANALYSIS OF GROUND DEFLECTION AND SETTLEMENT DUE TO DIAPHRAGM WALL INSTALLATION: A CASE STUDY AT EGYPTIAN METRO STATION

Gihan E. Abdelrahman, Mohammed H. AbdelAziz, Abdelrahman E. Sayed¹

Civil Engineering. Dept., Faculty of Engineering, Al-Fayoum University, Al Fayoum, 63514, Egypt.

* Correspondence: ai1104@fayoum.edu.eg

Citation:

G. E. Abdelrahman, M. H. AbdelAziz, A. E. Sayed "Numerical Analysis of Ground Deflection and Settlement Due to Diaphragm Wall Installation: A Case Study at Egyptian Metro Station", Journal of Al-Azhar University Engineering Sector, vol. 20(77), pp. 1453-1473, 2025.

Received: 19 April 2025 Revised: 15 June 2025 Accepted: 01 July 2025

Doi: 10.21608/auej.2025.386739.1844

Copyright © 2025 by the authors. This article is an open access article distributed under the terms and conditions Creative Commons Attribution-Share Alike 4.0 International Public License (CC BY-SA 4.0)

ABSTRACT

This study investigates ground movements resulting from diaphragm wall (D-wall) excavation during the construction of an underground metro station in Heliopolis, Cairo. In a densely populated urban environment, horizontal soil displacement and additional pressure on support systems present major geotechnical concerns. Influencing factors include subsurface conditions, excavation depth, wall stiffness, construction sequence, nearby infrastructure, and surface loading. Field data collected over two years were analyzed and compared with numerical simulations using both Mohr-Coulomb and Hardening Soil models through two-dimensional (2D) and three-dimensional (3D) finite element methods. The study aims to assess the predictive accuracy of these models and evaluate the potential risks to surrounding structures. Findings indicate maximum horizontal wall displacements between 0.04% and 0.06% of excavation depth, with surface settlements ranging from 6% to 32% of lateral wall movement. The outcomes enhance understanding of soil-structure interaction and contribute to safer design, planning, and monitoring of deep excavations in urban metro development.

KEYWORDS: Deep excavation, Diaphragm wall, Lateral wall deformation, Finite element analysis and Surface settlement.

التحليل العدي لتشكل وهبوط الارض الناتج عن حائط الديفرام وول: حالة الدراسة في محطة مترو مصرية

جيهان السيد عبدالرحمن، محمد حسين، عبدالرحمن ابراهيم سيد*

قسم الهندسة المدنية، كلية الهندسة، جامعة الفيوم، القاهرة، ٦٣٥١٤، مصر البريد الالكتروني للباحث الرئيسي: ai1104@fayoum.edu.eg

الملخص

تُعنى هذه الدراسة بتحليل الحركات الأرضية الناتجة عن أعمال حفر جدران الحجاب (Diaphragm Wall) خلال تنفيذ محطة مترو أنفاق تحت الأرض في منطقة هليوبوليس بمدينة القاهرة. في ظل الكثافة العمرانية العالية، تُعد الإزاحات الأفقية للتربة والضغوط الإضافية على أنظمة الدعم من أبرز التحديات الجيوتقنية التي تواجه تنفيذ مثل هذه المشاريع. وتتأثر هذه التشكلات بعدة عوامل، من بينها الخصائص الجيولوجية للتربة، عمق الحفر، صلابة الجدران الساندة، تسلسل التنفيذ، قرب المنشآت المجاورة، والأحمال السطحية. تم إجراء تحليل لبيانات رصد ميداني جُمعت على مدار عامين، ومقارنتها بنتائج نماذج عددية باستخدام نماذج مو هركولومب (Mohr-Coulomb) والتربة المتصلبة (Hardening Soil) ، وذلك من خلال تطبيق منهجية العناصر المحدودة في بعدين

الكلمات المفتاحية: الحفر العميق، الحانط الحاجز، التشكل الجانبي للجدارن، التحليل بالعناصر المحددة، هبوط سطح الأرض.

1. INTRODUCTION

The increasing scarcity of surface space in major urban centers has resulted in complex traffic systems and intensified transportation demands. In response to these challenges, underground construction has emerged as a strategic solution to alleviate surface congestion and expand usable urban infrastructure. In Cairo a city recognized as one of the most densely populated not only in Egypt but globally such developments have been essential. The expansion of the Cairo Metro Line 3 (CML3), which stretches from Imbaba to Cairo International Airport, represents a key effort to enhance urban mobility. Specifically, Phase 4A of CML3 extends approximately 5.1 kilometers, from Heliopolis Station to the Exit Shaft. The general layout of Heliopolis Station, which serves as the focal point of this study, is part of this effort to alleviate the growing transportation demand. In tunneling projects, a primary engineering objective is to minimize ground surface settlement resulting from excavation activities.

The foremost concern in such operations is often the prevention of excavation collapse [1,2]. Accurately estimating the maximum surface settlement is essential, as it supports the nonlinear calibration of input parameters across multiple observational targets. However, the reliability of stability assessments is closely tied to the accuracy of the soil behavior representation within the chosen numerical simulation model. In densely populated urban environments, deep excavations are often carried out in close proximity to existing structures. Such activities can lead to unanticipated ground movements, posing a significant risk of damage to nearby buildings. The behavior of retaining walls and the deformation of surrounding soil have been extensively investigated in past studies [3-6].

These investigations commonly employ the Finite Element Method (FEM) to model and predict subsurface ground responses resulting from excavation processes. Many researchers have relied on the Finite Element Method (FEM) to model subsurface ground variations resulting from excavation activities. Field measurements have confirmed that ground movement induced by diaphragm wall installation can represent a significant portion of overall soil displacement [7,8]. A study approach, combining 3D nonlinear analysis due to unexpected deflection values with a constitutive model to account for variations in bulk and shear moduli based on stress loading scales, was proposed by Comodromos et al. [9]. It was observed that the most substantial ground movement occurs at the onset of panel installation, with lateral movements in subsequent panels being notably reduced. Hsiung and Dao [10] emphasized that more accurate predictions of ground surface settlements can be achieved by adopting advanced constitutive models that incorporate the small strain characteristics of soil in numerical analyses.

By utilizing such models, engineers can better predict ground surface settlements while considering the soil's response at small strains. However, the input parameters for these models often require complex and detailed testing. In the present study, the authors assessed the applicability of their predictive model by comparing its results with observed field data. Due to unexpected deflection values recorded in the diaphragm walls, the authors recommend a comprehensive soil characterization to better understand the subsoil conditions. This approach will help delineate the failure zones within the soil and mitigate the risk of future damage at Heliopolis Station, thereby reducing potential hazards.

2. CASE STUDY

This section presents an overview of the project, including its main features, the site's soil conditions, the sequence of construction stages, and the field measurements conducted to monitor performance and validate design assumptions.

2.1. Project Description

Cairo is one of the most populous cities in the world. Several years ago, the Egyptian government began the development of a metro transportation network, leading to the creation of the Cairo Metro system. The system currently comprises three operational lines: Line 1 (the main line), Line 2, and Line 3, with a fourth line still under construction. This study focuses on Line 3, which consists of 27 stations. Specifically, we investigate the Heliopolis Tunneling Station, one of the largest metro stations in both the Middle East and Africa. The station spans from Haroun to El Nozha 1. Fig. 1 presents the station layout, which includes two intersecting rectangular plots in phases 4A and 4C, with approximate dimensions of 225 m by 23 m. The excavation dimensions for this station are 20.74 m in width, 225 m in length, and approximately 28.5 m in depth. Fig. 2 illustrates the static crosssectional system of the specified case, which features a rectangular diaphragm wall with a depth of 41 meters and a thickness of 1.20 meters. The wall is supported by four levels of reinforced concrete slabs constructed sequentially: the roof slab, ticket slab, intermediate slab, and raft slab. These slabs provide lateral support to the diaphragm wall at different excavation stages. Additionally, a series of temporary inclined struts, spaced approximately every 3 meters horizontally, are installed between the intermediate and raft foundation. These struts enhance the wall's stability at deeper levels, as shown in **Fig.2**.

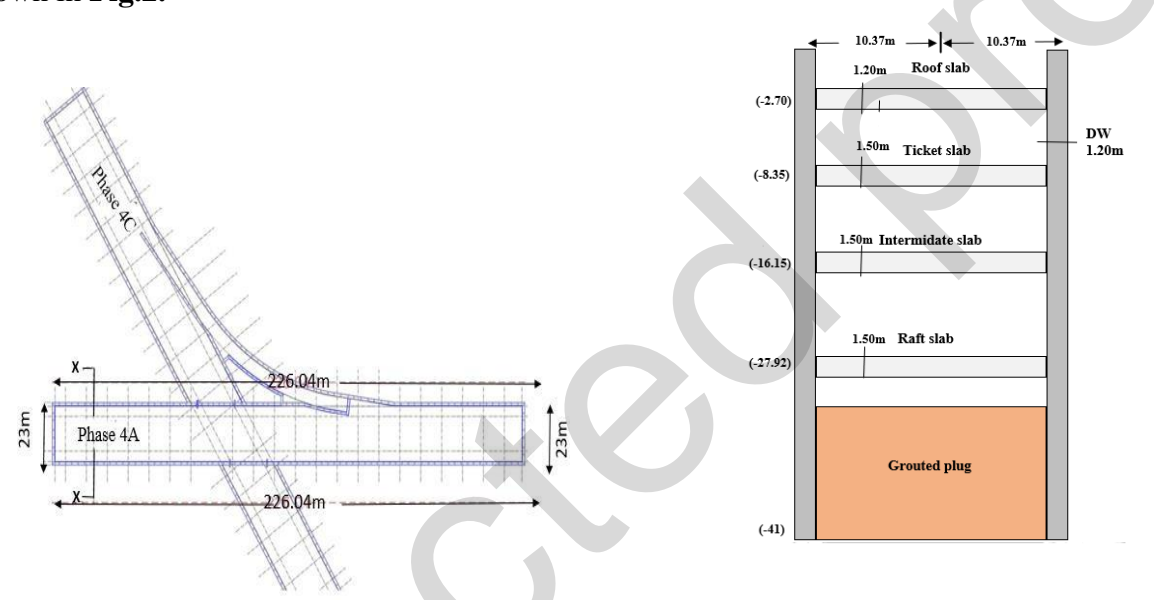


Fig. 1: Layout of Heliopolis Underground Station

Fig. 2: Cross Section X-X in Heliopolis Station

2.2. Soil Profile

Fig. 3 and **Fig. 4** depict locations and the specifics of Bore hole with standard penetration test, which used in this case study. The underground water level is -28.30 m under the ground surface, according to the results of in-situ and laboratory investigations. Soil stratification is defined as follows: Layer (1) a two- meter-thick layer emerged at elevations ranging about 2m. This stratum is fill contains asphalt, sand, gritty gravel and sand with gravel. Layer (2) following the fill top layer, the thickness about 9.80m. This layer is dense to very dense, fine to coarse sand and gravel, with traces of silt and calcareous. Layer (3) the thickness of the subsequent layer is altered 9.20m. This layer is stiff, silty clay. The liquid limit, plasticity index and water content are 54%, 21% and 22%, individually. Layer(4) the thickness of the subsequent layer is 29.5m, this layer is dense sand.

Heliopolis Staion

Fig. 3: Soil Lithology locations BH 103 & 104

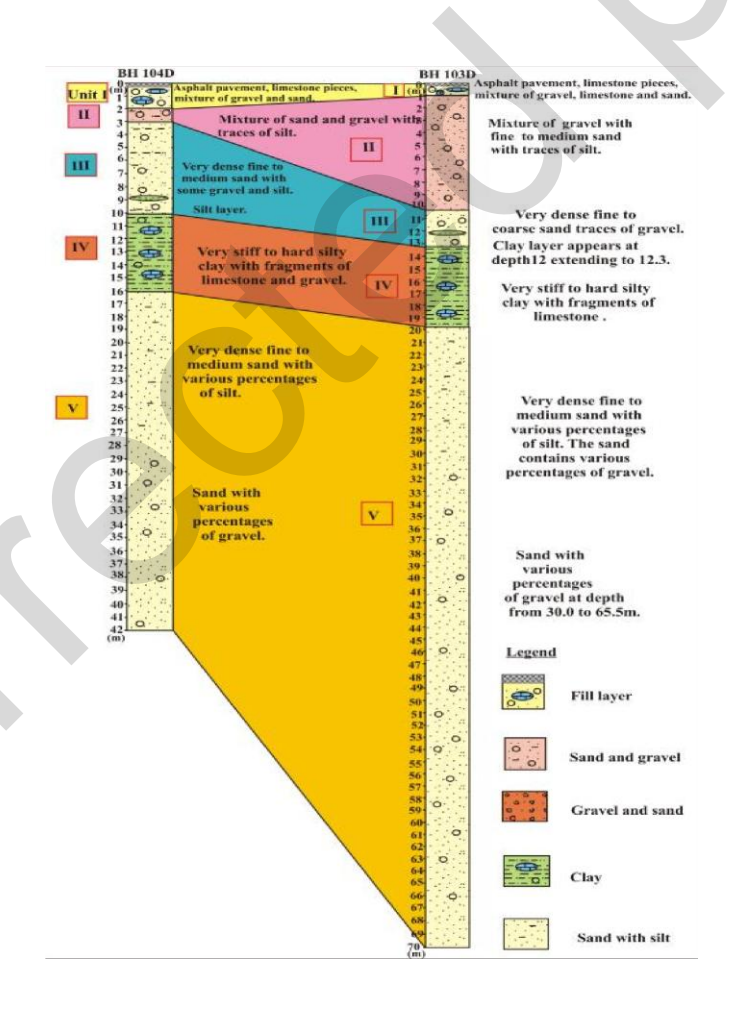


Fig. 4: Soil Lithology BH 103&104

2.3. Construction Stages

Fig. 5 depicts the methodology of top-down works used in the construction of station [11]. First, install a diaphragm wall around the station, as indicated in **Fig. 5.a**. Second, as indicated in **Fig. 5.b**, soil injection is used to create a non-porous pluge under the raft. Third, as indicated in **Fig. 4.c**, excavate beneath the roof slab to construct a concrete roof slab. Fourth, as illustrated in **Fig. 5.d**, excavate beneath the ticket slab to construct the concrete ticket slab. Fifth, as indicated in **Fig. 5.e**, excavate beneath intermediate slab to construct a concrete intermediate slab. Six, excavation understeel inclined strut supports, as illustrated in **Fig. 5.f** to create the inclined steel struts. Seventh, excavate beneath the raft slab to construct a concrete raft slab, as indicated in **Fig. 5.g**. Eight, as illustrated in **Fig. 5.h**, remove the inclined struts.

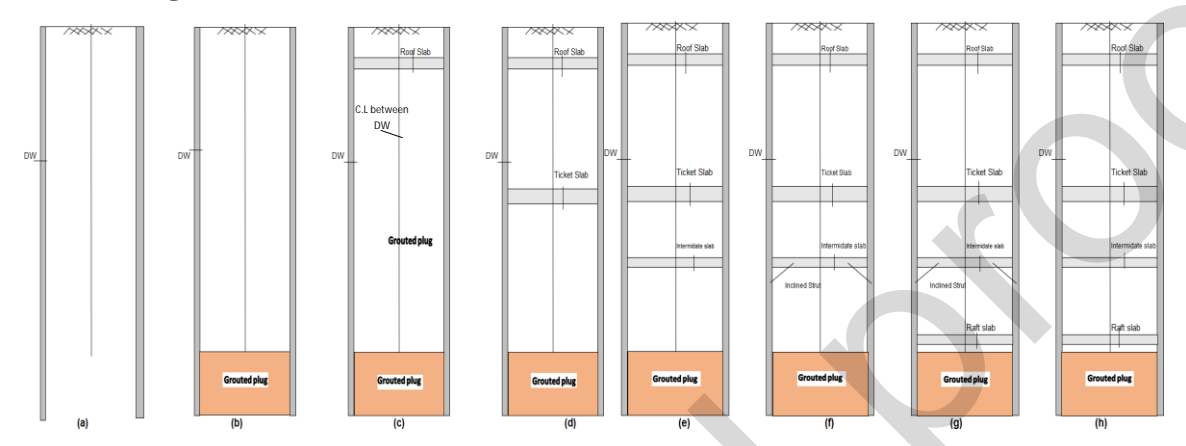


Fig. 5: Stages of adopted construction of deep excavation system

2.4. Field Measurement

To measure the actual field deformation during the top-down diaphragm wall construction, inclinometer devices were installed along the panels of the station, as shown in **Fig. 6**. It is important to note that the inclinometer readings (1) were taken after the completion of the station construction stages. The final four readings indicate a stabilization of the measurements, with the maximum lateral deformation of the wall recorded at 16.58 mm, as illustrated in **Fig. 6**.

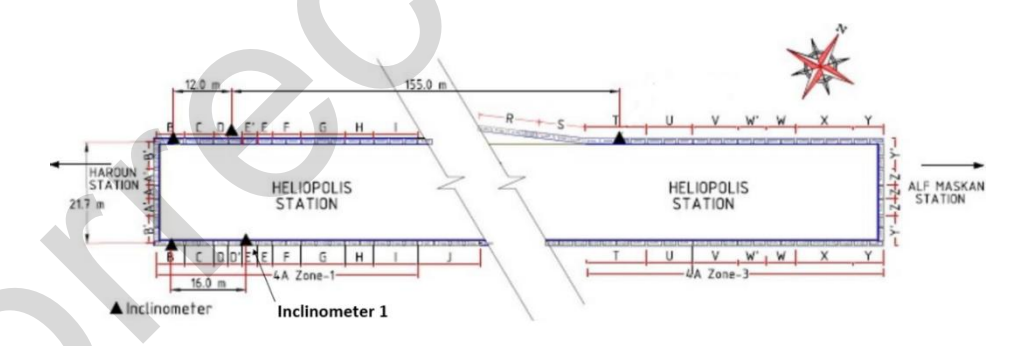


Fig. 6: Inclinometer locations of Station phase (4A)

3. ANALYSIS METHOD OF NUMERICAL MODEL

This research utilized Plaxis 2D&3D as the primary software for conducting numerical analyses. Two different soil constitutive models were employed—namely, the Mohr-Coulomb (MC), Hardening Soil (HS) to represent the soil layers and assess their effectiveness in forecasting wall deformations, and surface settlements caused by station construction. While all models shared identical strength parameters, their stiffness parameters varied. In the MC model, stiffness values were fixed, whereas

in the HS models, it depended on stress levels. As a consequence, the lateral deformation and settlement results of both numerical models (2D and 3D) are compared to field measurements in **Fig. 7**.

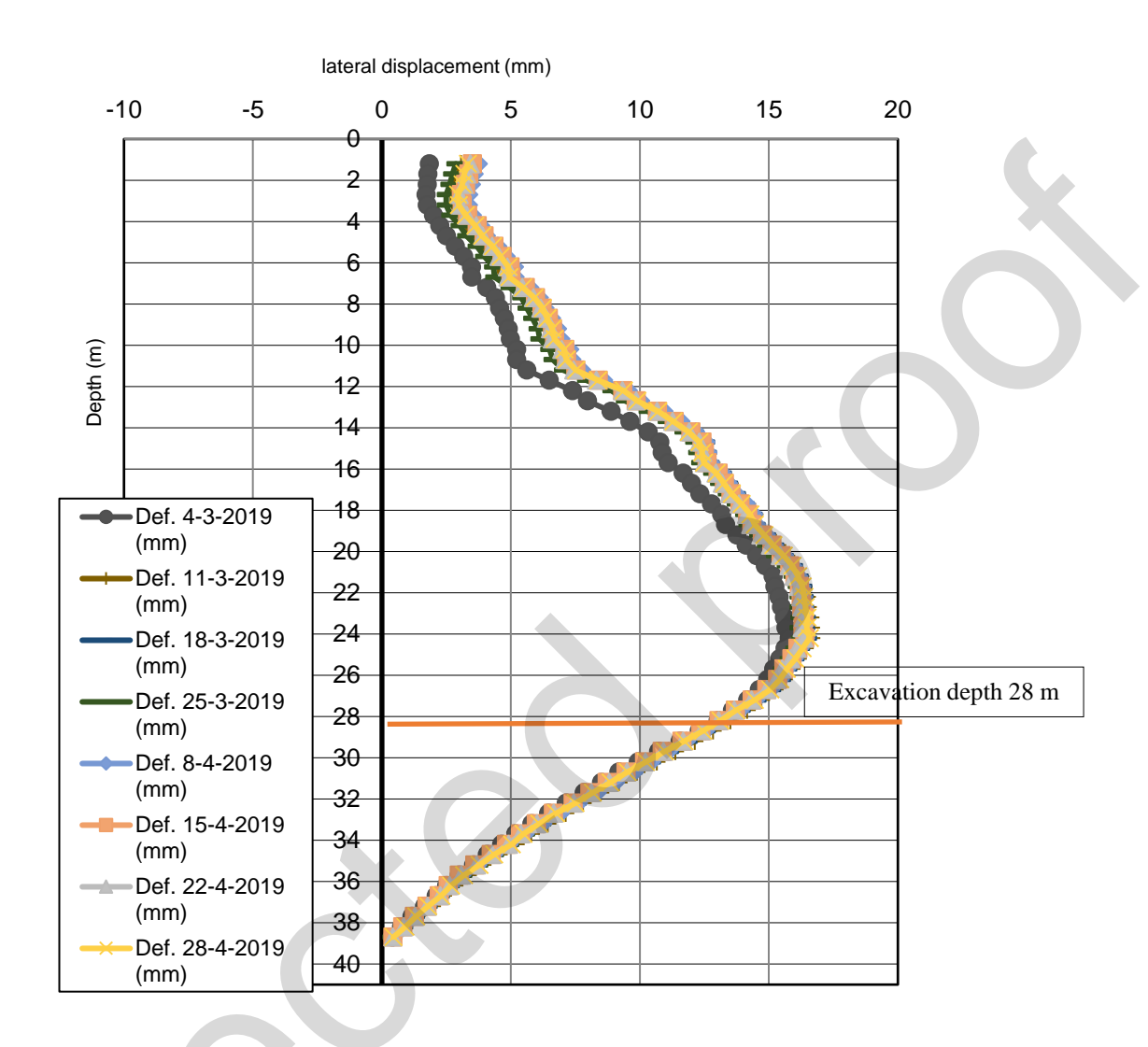


Fig. 7: Last measurements of Inclinometer (1) at Year 2019

3.1. Method Settlement and Adapted Constitutive Models

Soils exhibit non-linear behavior when subjected to variations in strain or stress, with their stiffness being influenced by several factors, including the applied stress state, the loading path, and the strain level. The Mohr-Coulomb (MC) model, which is a basic linear elastic model, assumes completely plastic behavior following yielding, making it suitable for preliminary evaluations based on isotropic elasticity, as described by Hooke's law. This model is often used in cases where simplification is required for initial design or analysis. In contrast, the Hardening Soil (HS) model, proposed by Schanz et al. (1998), offers a more advanced approach for modeling the behavior of soils, ranging from soft to hard materials. The HS model accounts for the reduction in stiffness and the development of irreversible plastic strains under primary deviatoric loading. Unlike the MC model, the HS model incorporates plasticity theory, improving upon the hyperbolic model, which is based solely on elasticity. The HS model also incorporates soil dilatancy and introduces a yield surface, enabling it to better capture the non-linear stress-strain behavior of soils during loading and unloading phases. This model represents soil behavior using three distinct stress-dependent moduli: the oedometer modulus (Eoed), the secant modulus at 50% of the maximum stress (E50), and the unloading/reloading modulus (Eur). These moduli are essential for capturing the highly non-linear relationship between stress and strain during the initial loading phase, as well as for modeling the unloading effects [11].

For the MC model, stiffness parameters are typically derived from correlations with the Standard Penetration Test (SPT) N-values [12]. For the HS model, the stiffness moduli are defined as follows in **Equation (1)** and **Equation (2)**:

$$E_{50} = E_{OED} = E'$$
 Eq (1)

Where represents the stiffness parameter used in the MC model.

$$E_{ur} = 3E_{50}$$
 Eq (2)

Where representing the unloading/reloading modulus, which is three times the E50 value.

The stress-level dependency of stiffness is described by the relationship

$$m = 0.45 + 0.003Dr(\%)$$
 Eq (3)

where Dr is the relative density of the soil, as established by Teo and Wong [13].

Table 1 shows the main basic parameters for the two models related by the soil layers.

Table 1: Soil Data Sets Parameters

Dept	th (m)										MC		I	IS	
From	To	Soil layer	SPT N60	γsat (kN/m3)	с' (кРа)	0,0	(-) 1	K_o	(W)	(Rinter) (-)	E' (kN/m2) *10^3	E50 (kN/m2) *10^3	Eoed (kN/m2) *10^3	Eur (kN/m2) *10^3	m (-)
0	-2	Fill	32	18	1	27	0.3	0.37	-	.67	15	15	15	45	0.55
-2	- 11.80	Sand	50	19	1	37	0.3	0.24	7	.67	75	75	75	225	0.55
-11.80	-21	Clay	37	19	15	29	0.35	0.34	-	.67	40.5	40.5	40.5	121.5	0.55
-21	-50	Dense Sand	75	21	1	42	0.3	0.19	12	.67	120	120	120	360	0.7

3.2.2D&3D Numerical Model Geometry

The two-dimensional finite element method (2D FEM) proves to be particularly advantageous in geotechnical engineering applications where the primary focus lies on horizontal ground surfaces. In this study, the subsurface soil strata were modeled using high-order 15-noded two-dimensional elements, allowing for accurate representation of the soil behavior. Structural components such as diaphragm walls and concrete slabs were simulated using plate elements to adequately capture their flexural response. Numerical model was configured with dimensions of 115 meters in width and 96 meters in depth, as illustrated in **Fig. 8.** The 3D model is used to represent the whole geometry of soil structure. providing a more realistic depiction of field condition. The 3D FM model's soil layers are represented by high order 10-noded mesh elements with the same mesh and dimensions which used in 2D model as shown in **Fig. 9**.

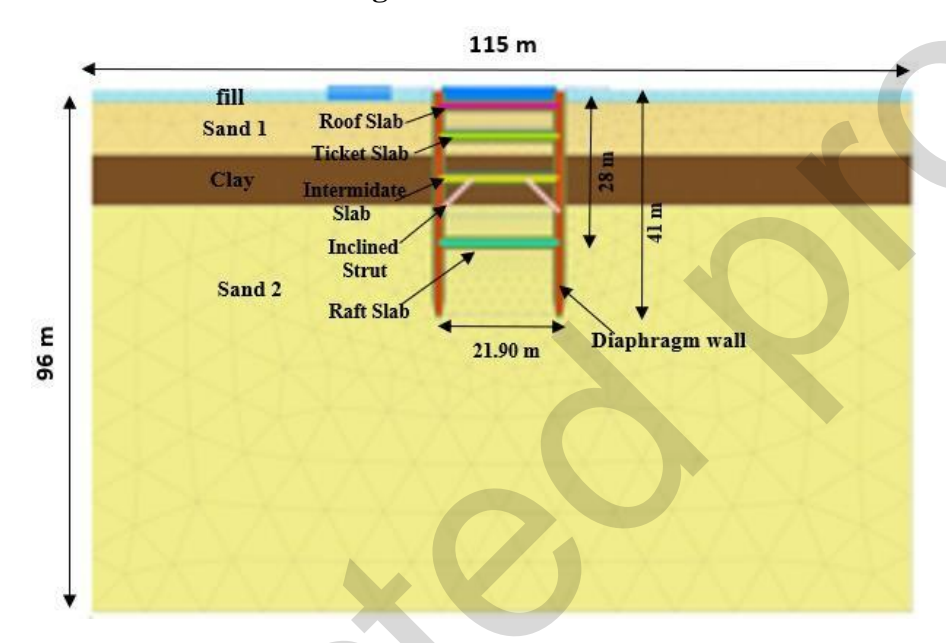


Fig. 8: Geometry of 2D FE Model

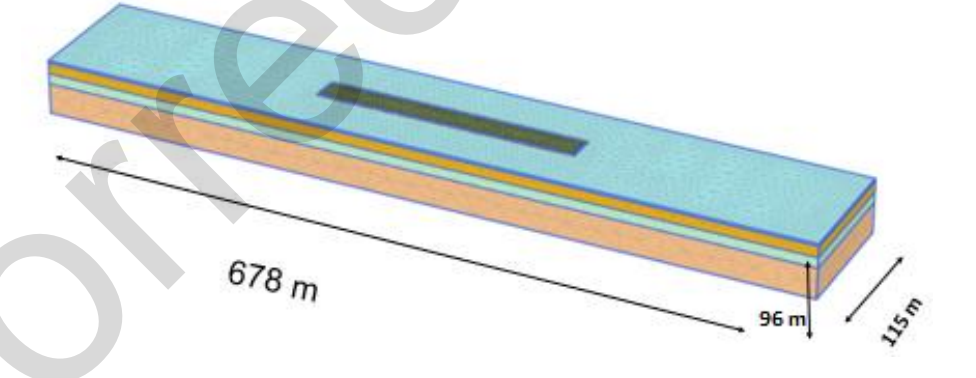


Fig. 9: Dimension and boundary of 3D FE Model

3.3.Design considerations

Finite element analyses were carried out using PLAXIS 2D and PLAXIS 3D to model the structural response of various components within the excavation support system during the construction of the underground metro station. The diaphragm wall (D-wall), structural columns, roof slab, concourse slab, and base slab were modeled as plate elements to adequately capture their flexural stiffness and membrane behavior. The elastic modulus E for these components was assigned based on characteristic concrete grades, with M40 used for the D-wall and M35 for all slab elements,

consistent with standard design specifications [14]. To reflect field conditions more accurately, a 20% reduction in the effective strength of the diaphragm wall was introduced. This adjustment accounts for quality degradation typically observed in tremie concrete placement, particularly under submerged conditions or in deep trench environments [15]. Temporary steel struts, designed to resist axial forces generated by lateral earth pressures during excavation stages, were simulated using node-to-node anchor elements with axial stiffness properties calibrated according to typical steel bracing design practice [16]. The excavation sequence and support installation were modeled in a staged construction framework, enabling detailed evaluation of stress redistribution, wall deflections, and structural forces at each excavation level. **Table 2** summarizes key structural properties of various slab elements used in the design of a substructure, including diaphragm walls (D-walls), roof slabs, ticket level slabs, intermediate slabs, and raft foundations. For each slab, important parameters such as thickness, axial stiffness (EA), flexural stiffness (EI), unit weight, and Poisson's ratio are provided. These properties are essential for accurate structural modeling and analysis.

Table 2: Material properties for Structure elements and design considerations

Thickness	Identification	Axial force (EA)	Flexural stiffness (EI)	weight (w)	Poisson's ratio (v)			
(m)	of slab	(kN/m)	(kNm²/m)	(kN/m/ m)	(-)			
1.2	D-Wall Continuous	2.39E+07	2.87E+06	30	0.2			
1.2	Roof Continuous	2.80E+07	3.36E+06	25	0.2			
1.5	Ticket & Intermediate	3.50E+07	6.56E+06	25	0.2			
	Continuous							
1.5	Raft Continuous	3.50E+07	6.56E+06	25	0.2			
Surcharge	Construction loads	Uniform surcharge of 20 kPa for 2m width is directly applied on the ground level.						
Ground		Full water table at ground level has been considered in the analyses behind the diaphragm wall.						
water table		The water table is modelled 1m below the excavated level for the excavation side.						
Surcharge		Uniform surcharge of 50 kPa with minimum 20 m width behind.						
	Building loads	the excavation has been applied on the active side (1.5 m below ground level) of the retaining system.						
	Vehicular loads	Minimum 20 kPa surcharge above station box and entrances if any, is applied after backfillin to ground level.						

4. Ground Surface Settlement

This part presents real measured settlement data from nearby buildings to evaluate actual ground movements during construction. It then estimates the ground surface settlement using the Peak Method, which relies on empirical formulas. Finally, a numerical study is conducted to predict settlement, comparing these results with both measured data and analytical estimates for accuracy.

4.1 Settlement Real Measured Data for Surrounding Buildings

This study investigated six buildings with in the Heliopolis station's influence zone: Hel 2, Hel 8, Hel 9, Hel 18, Hel 23, and Hel 25 as in Fig. 10. The Elevation Reference Point (ERP) technique was applied to monitor vertical movements in these structures. Time-displacement graphs were generated to track soil movement over time, with the results for the respective ERP points shown in **Fig. 11** and **Fig. 12**. During the pre-drilling phase, elevating the ground level near the excavation perimeter significantly influences the upper soil layers, often resulting in a loss of captured data related to surface displacements due to construction activities. Vertical displacements at greater depths are particularly critical, especially for structures with deep foundations. This phenomenon may be attributed to the reduced influence zone, which is approximately half the depth of the excavation (Aye et al., 2006). The displacement monitoring in this study commenced in August 2016 and concluded in May 2019, covering a duration of over two years. The recorded data exhibited variability both between buildings and at different monitoring points within the same building. For instance, at point "a" of building Hel 2, there was a slight increase in subsidence over time (Fig. 11a), whereas a more pronounced displacement was observed at corner "A" of the same structure. In contrast, corner point "A" of building Hel 23 demonstrated a consistent increase in displacement, beginning in May 2017 and continuing thereafter (**Fig. 12c**). For building Hel 18, a stabilization in settlement was observed after November 2019 at points "A," "B," and "C" (Fig. **12a**). **Table 3** indicates the max measured settlements for surrounding buildings.

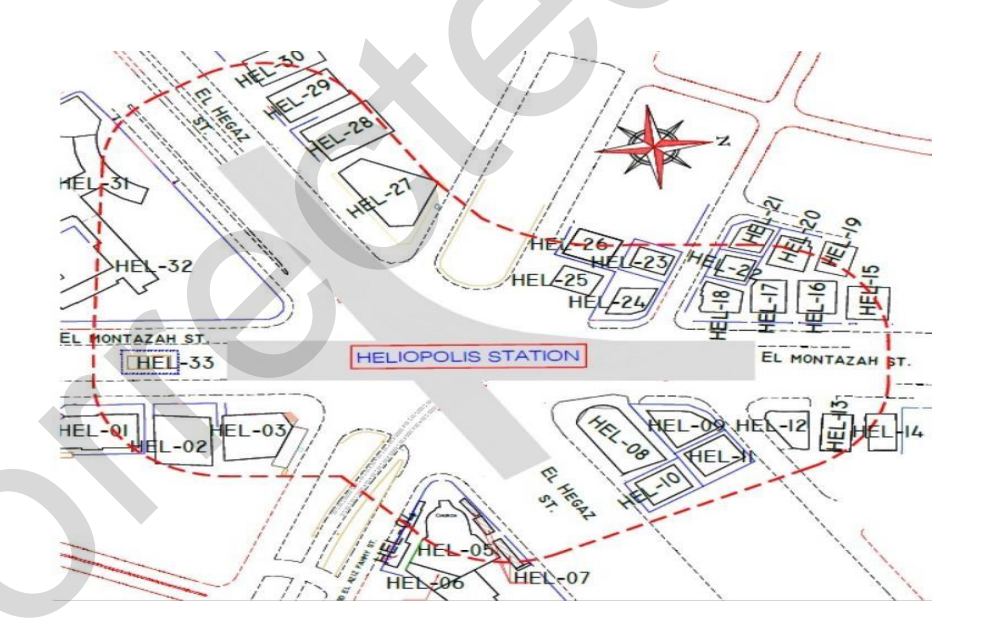


Fig. 10: General layout of Heliopolis Station

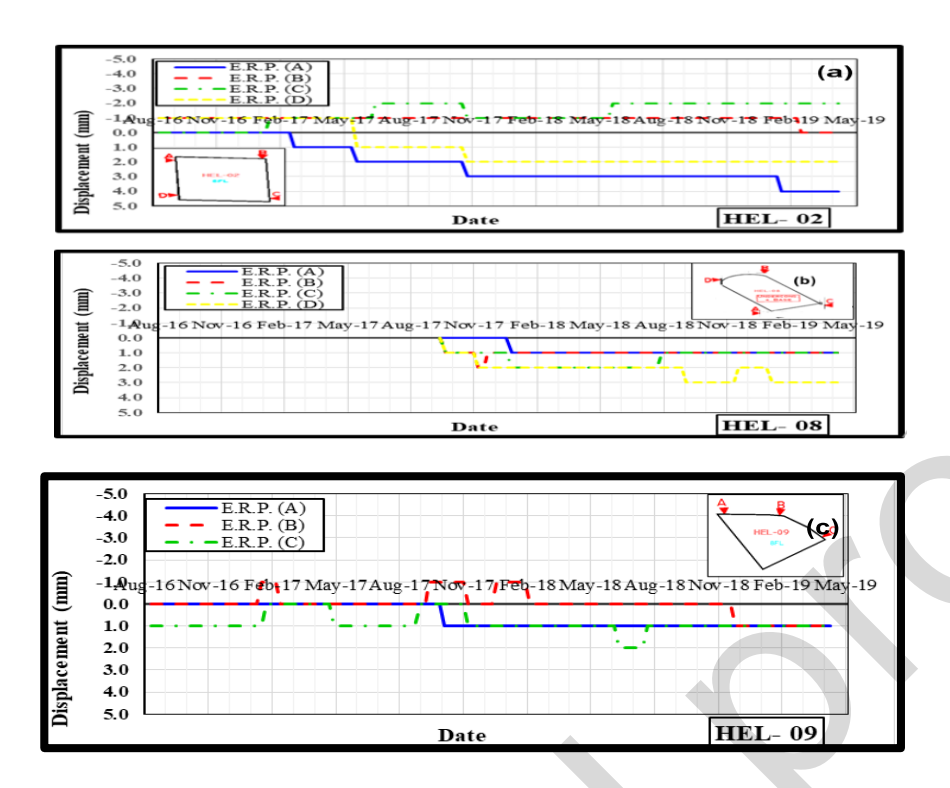


Fig. 11: Site monitoring of time-settlement relationships was conducted for elevated reference points at the following buildings under observation: a) HEL 2, b) HEL 8, and c) HEL 9

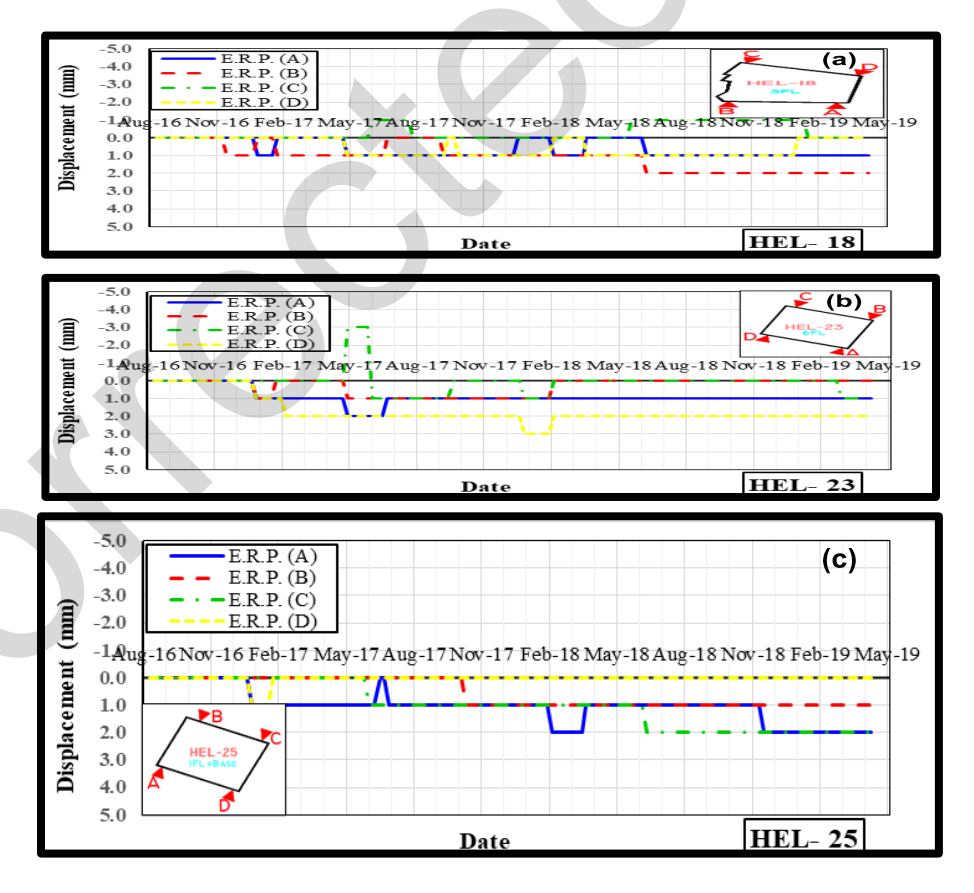


Fig. 12: Time-settlement relationships for elevated reference sites under observation for: Buildings in a) HEL 18, b) HEL 23, and c) HEL 25

Table 3: Max monitoring settlement for Surrounding Building

Surrounding Building	Max. actual Settlement (mm)
HEL02 point(A)	4
HEL08 point(D)	3
HEL09 point(C)	1
HEL18 point(A)	2
HEL23 point(D)	2
HEL25 point(A)	2

4.2 Estimating of Ground Settlement Surface (Peak method)

In order to estimate the ground settlement induced by diaphragm wall construction, the methodology adopted in this study is based on empirical models derived from field observations, particularly those proposed by Peck (1969). The total settlement is considered as the combination of two primary components: the settlement caused by trenching for diaphragm wall installation, and the settlement resulting from subsequent excavation behind the wall.

The maximum vertical settlement S_{max} at the ground surface is estimated as a proportion of the final excavation depth H, using the following empirical relationship as in **Equation** (4):

$$S_{max} = \alpha. H$$
 Eq (4)

Where:

 (α) is a coefficient dependent on soil type and construction technique, typically ranging between 0.001 and 0.01. Lower values of α are associated with stiffer soils (e.g., dense sands, stiff clays) and high-quality construction techniques (e.g., well-controlled slurry trenching and robust support systems), while higher values are often observed in softer soils and less controlled construction environments.

The total settlement at any point is obtained by summing the settlement components associated with wall trenching and deep excavation as **Equation** (5):

$$S_{total}(x) = S_{trenching}(x) + S_{excavation}(x)$$
 Eq (5)

Where

 $(S_{trenching}(x))$ is the settlement due to diaphragm wall trenching (typically shallow and localized),

 $(S_{excavation}(x))$ is the settlement due to deep excavation behind the wall (typically larger and more widespread).

1. Settlement Due to Diaphragm Wall Trenching $S_{trenching}$

This is typically shallow and localized settlement occurring during panel excavation and slurry support. It can be estimated as **Equation** (6):

$$S_{\text{trenching,max}} = \alpha_t. H$$
 $Eq(6)$

Where:

 (α_t) is the trenching settlement coefficient (typically 0.001–0.004, or 0.1–0.4% of excavation depth). Lower values are observed in dense granular soils or stiff clays with minimal soil loss, while higher values occur in soft clays or unstable trenching conditions.

(H) is the depth of the diaphragm wall trench (often the full depth of wall panel installation, even before excavation behind the wall).

Then the settlement at any distance x from the wall as in **Equation (7)**:

$$S_{\text{trenching}}(x) = S_{\text{trenching,max}} \cdot \exp\left(-\frac{x^2}{2i_t^2}\right)$$
 Eq (7)

Where i_t is the trenching settlement trough width, typically 0.3–0.5H.

2. Settlement Due to Excavation Behind the Wall Sexcavation

This is the more significant component and occurs after excavation starts behind the wall, causing wall deflection and ground movements. Estimated as **Equation (8)**:

$$S_{excavation,max}(x) = \alpha_{e}$$
. He Eq (8)

Where:

 (α_e) is the excavation settlement coefficient, typically 0.003–0.008 (or 0.3–0.8% of the final excavation depth),

(He) is the final depth of excavation behind the diaphragm wall as **Equation (9)**

$$S_{excavation}(x) = S_{excavation,max} \exp\left(-\frac{x^2}{2i_e^2}\right)$$
 Eq (9)

Table 4 shows the summary of the values of settlement coefficients related with the soil type.

Table 4: Values of settlement coefficients

Soil Type	Trenching Settlement Coefficient α t	Excavation Settlement Coefficient α e	Total Settlement Coefficient α	
Very stiff clay / Dense sand	0.001 – 0.002	0.003 - 0.004	0.004 - 0.006	
Stiff clay / Medium dense sand	0.0015 – 0.003	0.004 – 0.006	0.0055 – 0.009	
Soft clay / Loose sand	0.002 – 0.004	0.006 – 0.008	0.008 – 0.012	
Very soft clay / Organic soils	0.003 – 0.004	0.007 – 0.010+	0.010 – 0.014	

In order to estimate the ground settlement case study induced by diaphragm wall construction, which depth (H) is 41m, excavation depth (He) is 28m for the three buildings (HEL8 point (D)& HEL23 point (D)& HEL25 point (A)) at surface distance (x) from diaphragm wall $25.70\,m$, 45.70m and 31.40m respectively total settlement is considered as the sum of two primary

components: settlement due to diaphragm wall trenching and settlement caused by excavation behind the wall, as expressed in **Equation (5)**:

The trenching settlement is a localized effect occurring during panel excavation and slurry support, calculated by first determining the maximum settlement $S_{trenching,max}$ at the wall face using **Equation (6)**:

$$S_{\text{trenching,max}} = 0.0015 \times 41 = 0.0615 \,\text{m} = 61.5 \,\text{mm}$$

The settlement at any horizontal distance x from the wall is then given by **Equation (7)**: where i_t is the trenching settlement trough width, taken as 0.4 times the trench depth H, i.e.,

$$i_t = 0.4 \times 41 = 16.4 \,\mathrm{m}$$

The second component, settlement due to excavation behind the diaphragm wall, is generally more significant. Its maximum settlement $S_{excavation,max}$ is estimated from **Equation** (8):

where α_e is the excavation settlement coefficient, typically between 0.003 and 0.008, taken as .0035 was adopted

$$S_{excavation.max} = 0.0035 \times 280.0980 m = 98.0 mm$$

The excavation-induced settlement at any distance (x) is modeled by **Equation (9)**: with i_e as the excavation settlement trough width, assumed here as 0.5 times the excavation depth (He)

$$i_e = 0.5 \times 28 = 14.0m$$

For x = 25.70m

$$S_{\text{trenching}}(25.70) = 61.5 * \exp\left(-\frac{25.70^2}{2 * 16.4^2}\right) = 18.02 \, mm$$

 $S_{\text{excavation}}(25.70) = 98 * \exp\left(-\frac{25.70^2}{2 * 14^2}\right) = 18.26 \, mm$

$$S_{total}(25.70) = 18.02 + 18.26 = 36.28 \, mm$$

For x = 31.40 m

$$S_{\text{trenching}}(31.40) = 61.5 * \exp\left(-\frac{31.40^2}{2 * 16.4^2}\right) = 9.85 \ mm$$

$$S_{\text{excavation}}(31.40) = 98 * \exp\left(-\frac{31.40^2}{2 * 14^2}\right) = 7.95 \ mm$$

$$S_{total}(31.40) = 9.85 + 7.95 = 36.28 \, mm$$

For x = 45.70 m

$$S_{\text{trenching}}(45.70) = 61.5 * \exp\left(-\frac{45.70^2}{2 * 16.4^2}\right) = 1.26 \ mm$$

$$S_{\text{excavation}}(45.70) = 98 * \exp\left(-\frac{45.70^2}{2 * 14^2}\right) = .47 \text{ mm}$$

$$S_{\text{total}}(45.70) = 9.85 + 7.95 = 1.73 \text{ m}$$

These previous results indicate that settlement reduces with increasing distance from the diaphragm wall, dominated by excavation effects near the wall and diminishing significantly beyond 40 m. The methodology provides a reliable, field-validated approach for predicting settlements induced by diaphragm wall construction in dense granular soils. **Table 5** shows the Comparison of the Peak results and the measured data field.

Surrounding buildings	Distance (x) (m)	S _{trenching,max} (mm)	S _{excavation,max} (mm)	$S_{total}(x)$ (mm)	Max. actual Settlement (mm)
HEL08 point(D)	25.7	18.02	18.26	36.28	3
HEL23 point(D)	31.4	9.85	7.95	17.8	2
HEL25 point(A)	45.7	1.26	0.47	1.73	2

Table 5: Peak results and the measured data field.

4.3 Numerical Study for Predicted Settlement

A combination of three-dimensional Hardening Soil (HS) and Mohr-Coulomb (MC) models was employed to evaluate the settlement behavior of the surrounding buildings. The input parameters used for both models are identical and are provided in **Table 1**, based on consistent soil characteristics. **Fig 13** illustrates the spatial configuration of the surrounding structures incorporated into the 3D numerical simulation. The analysis focuses on three representative buildings HEL 8 (Point D), HEL 23 (Point D), and HEL 25 (Point A) located at horizontal distances of 25.7 m, 45.7 m, and 31.4 m, respectively, from the diaphragm wall. These cases were selected to highlight the differences between the numerically predicted and the actual measured settlements.

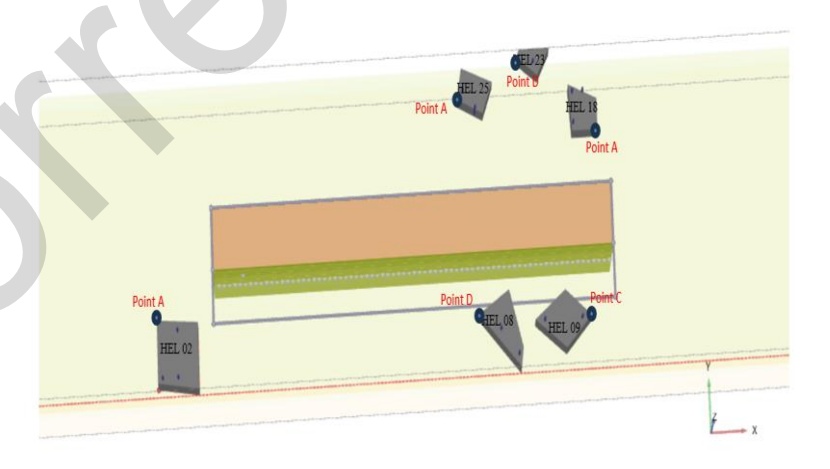


Fig. 13: 3D model for the surroundings building locations for the station of Heliopolis

5. RESULTS

This section presents the lateral deformation results, highlighting the horizontal displacements of retaining elements under various loading conditions. Section 5.2 introduces the Plane Strain Ratio (PSR), used to assess how closely the 2D plane strain model approximates real 3D behavior. Section 5.3 summarizes settlement results, focusing on vertical ground movement and its impact on surrounding structures and serviceability.

5.1.Lateral Deformation Results

Fig. 14 shows the 2D and 3D deformed shape results. **Fig.15a** illustrates the correlation between depth and lateral wall deformation based on the Mohr-Coulomb (MC) numerical models in both two-dimensional (2D) and three-dimensional (3D) analyses. For both 2D and 3D MC models, the peak lateral displacement is observed near the mid-height of the diaphragm wall. The maximum deformation predicted by the 2D MC model is 18.52 mm, which exceeds the field measurement by approximately 11%. In contrast, the 3D MC model estimates a maximum deformation of 15.13 mm, which is 8.74% lower than the observed field value. Similarly, **Fig.15b** presents the depth-lateral deformation relationship for the Hardening Soil (HS) model in both 2D and 3D forms. As with the MC models, the highest deformation in the HS models also occurs around the diaphragm wall's mid-height. The 3D HS model predicts the smallest lateral deformation, with a value of 12.442 mm, which is 24.90% less than the field measurement. Among the HS models, the 2D version shows a maximum lateral deformation that more closely aligns with the measured field inclinometer data, making it a more accurate representation in this context.

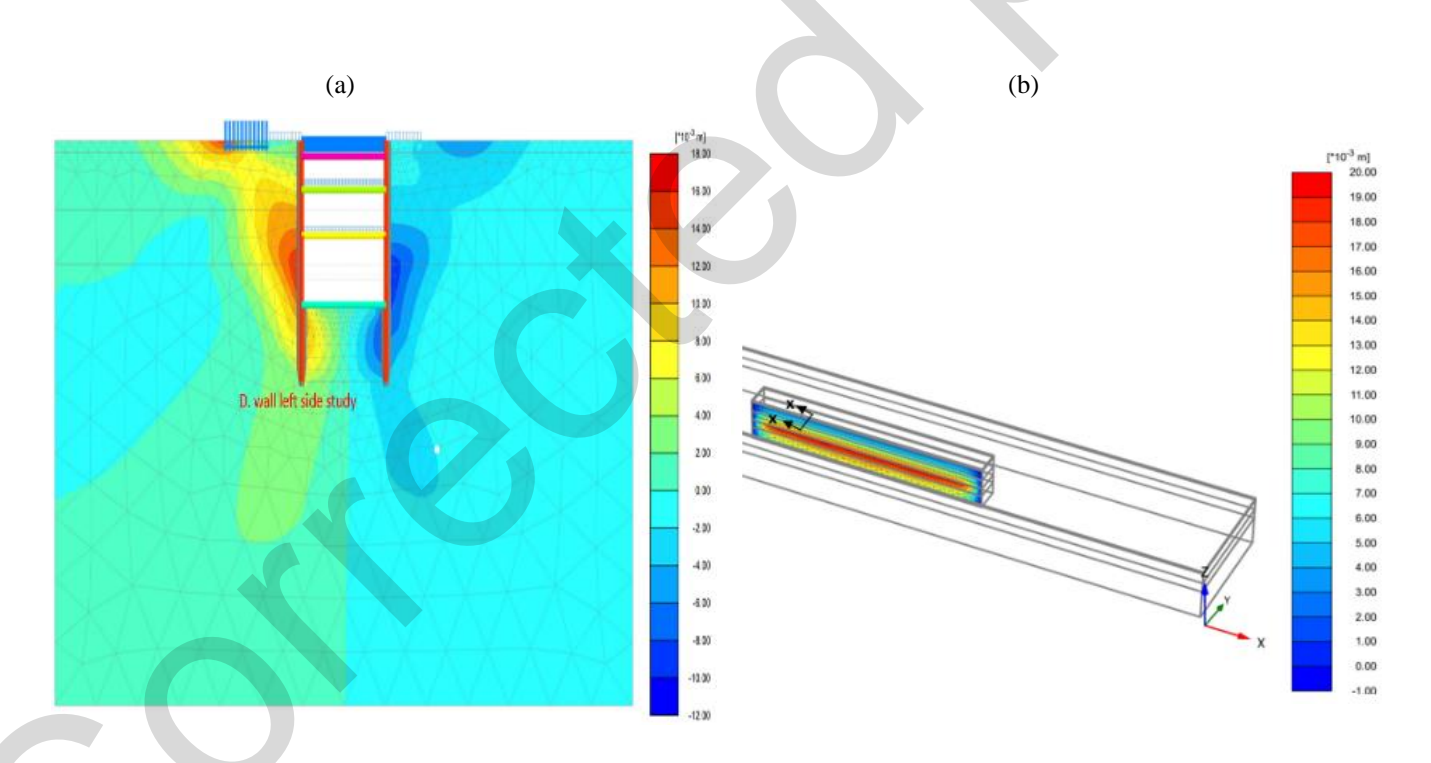


Fig. 14: Deformed shape (a) Two-dimensional model; (b) three-dimensional model

(a) (b)

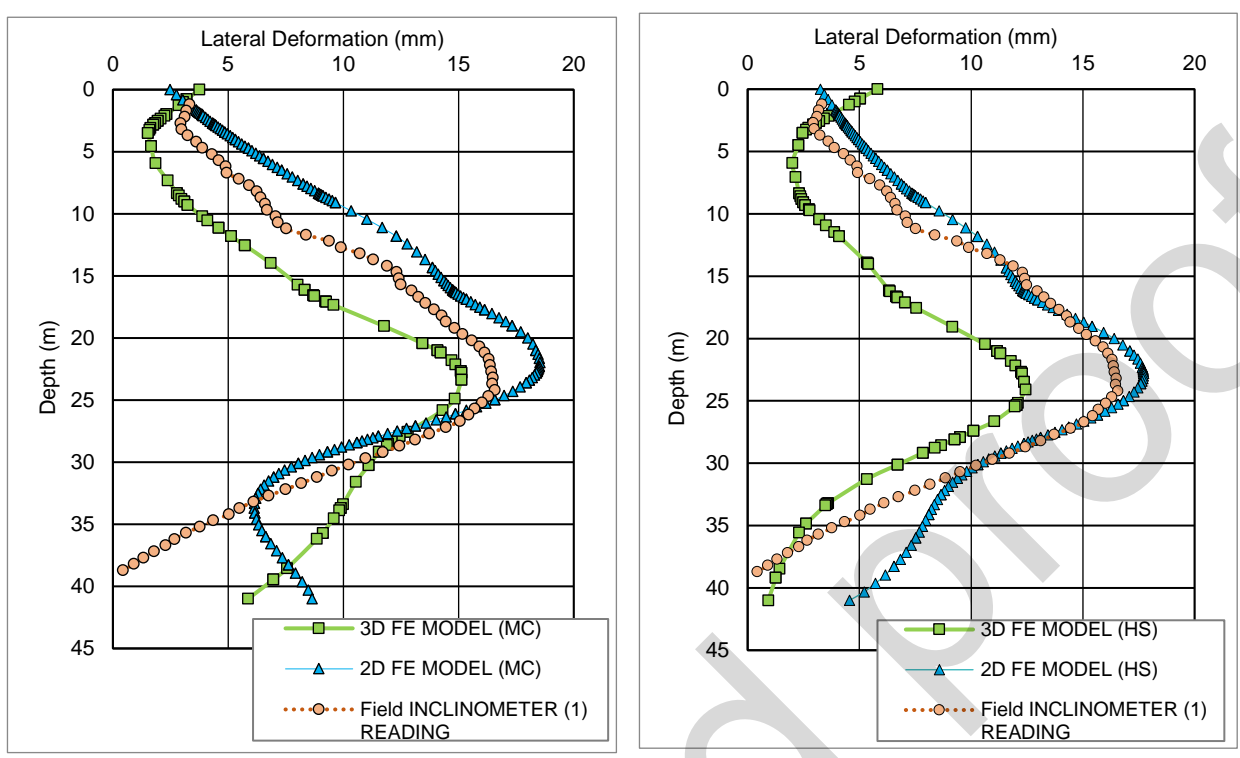


Fig 15: Comparison between field measurements and numerical simulation results: (a) Two-dimensional and three-dimensional Mohr-Coulomb (MC) models; (b) Two-dimensional and three-dimensional Hardening Soil (HS) models

5.2. Plane Strain Ratio (PSR)

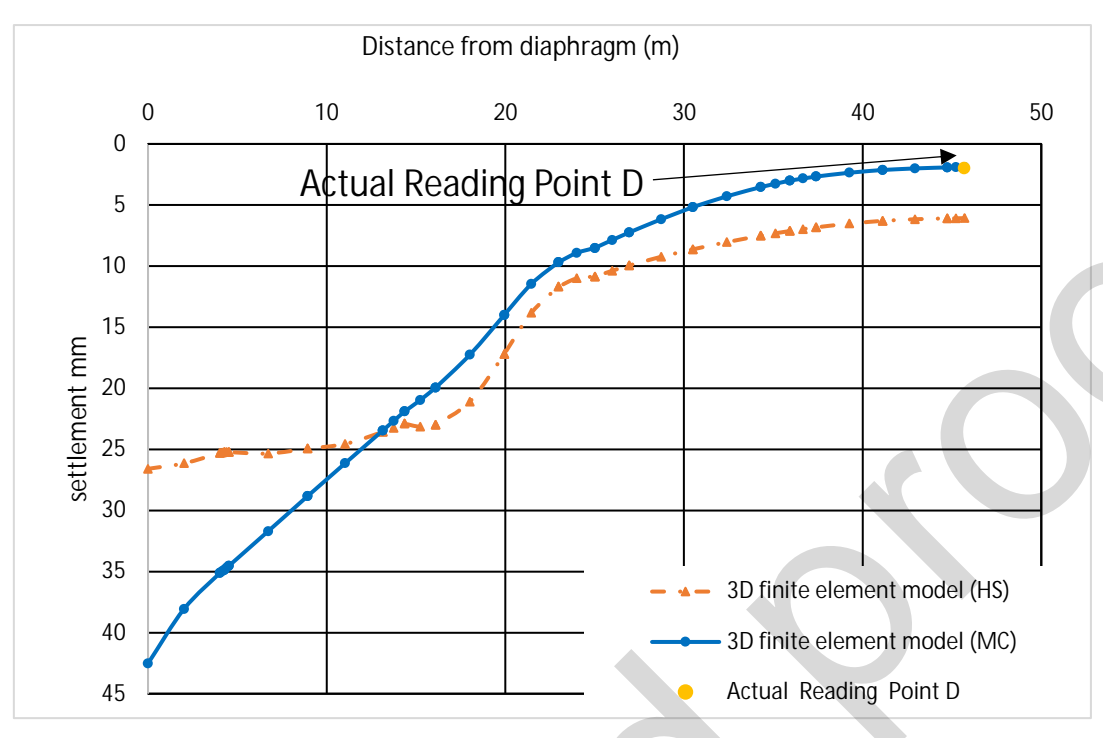
According to Finno et al. (2006) and Ou et al. (2006), the Plane Strain Ratio (PSR) is defined as the ratio of the maximum deflection predicted by a three-dimensional (3D) analysis to that obtained from a two-dimensional (2D) analysis. This study evaluates the PSR values for different soil constitutive models, to assess the influence of soil behavior on displacement predictions.

$$PSR = \frac{\text{Deflection computed via 3D analyses}}{\text{Deflections computed via 2D analyses}} Eq (10)$$

The calculated Plane Strain Ratio (PSR) for the Mohr-Coulomb (MC) model is approximately 0.956, while for the Hardening Soil (HS) model, it is approximately 0.702.

5.3. Settlement Results

Fig.16 presents the comparison between the measured ground settlement at point D of the HEL8 section and the predictions obtained from the 3D Hardening Soil (HS) and Mohr-Coulomb (MC) models. The 3D Mohr-Coulomb model provides the closest estimation, predicting a maximum settlement of 3.73 mm at a distance of 25.7 m from the diaphragm wall, which exceeds the measured settlement by approximately 19%. **Fig. 17** compares the measured ground settlement at Point D of the HEL23 section with the predictions generated by the 3D Hardening Soil (HS) and Mohr-Coulomb (MC) models. The 3D Mohr-Coulomb model produces an identical estimate, predicting a maximum settlement of 1.90 mm at a distance of 45.70 m from the diaphragm wall. Similarly, **Fig.18** illustrates the comparison for Point A of the HEL25 section. In this case, the 3D Mohr-Coulomb model again yields the closest approximation, predicting a maximum settlement of 5.23 mm at a distance of 31.40 m from the diaphragm wall, approximately 38% higher than the observed settlement. **Table 6** presents a comparison between the settlement results obtained from the 3D Mohr-Coulomb (MC) and 3D Hardening Soil (HS) models and the measured settlement values.



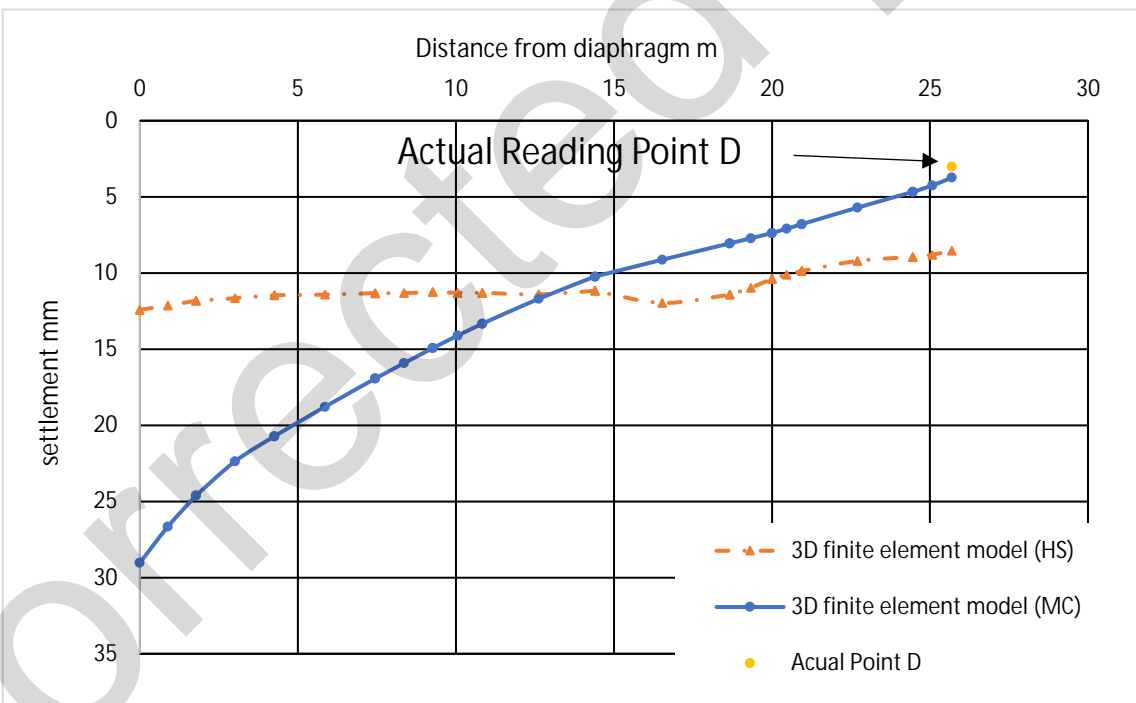


Fig. 16: 3D HS & MC The predicted settlement at the location of HEL8

Fig. 17: 3D HS & MC The predicted settlement at the location of HEL23

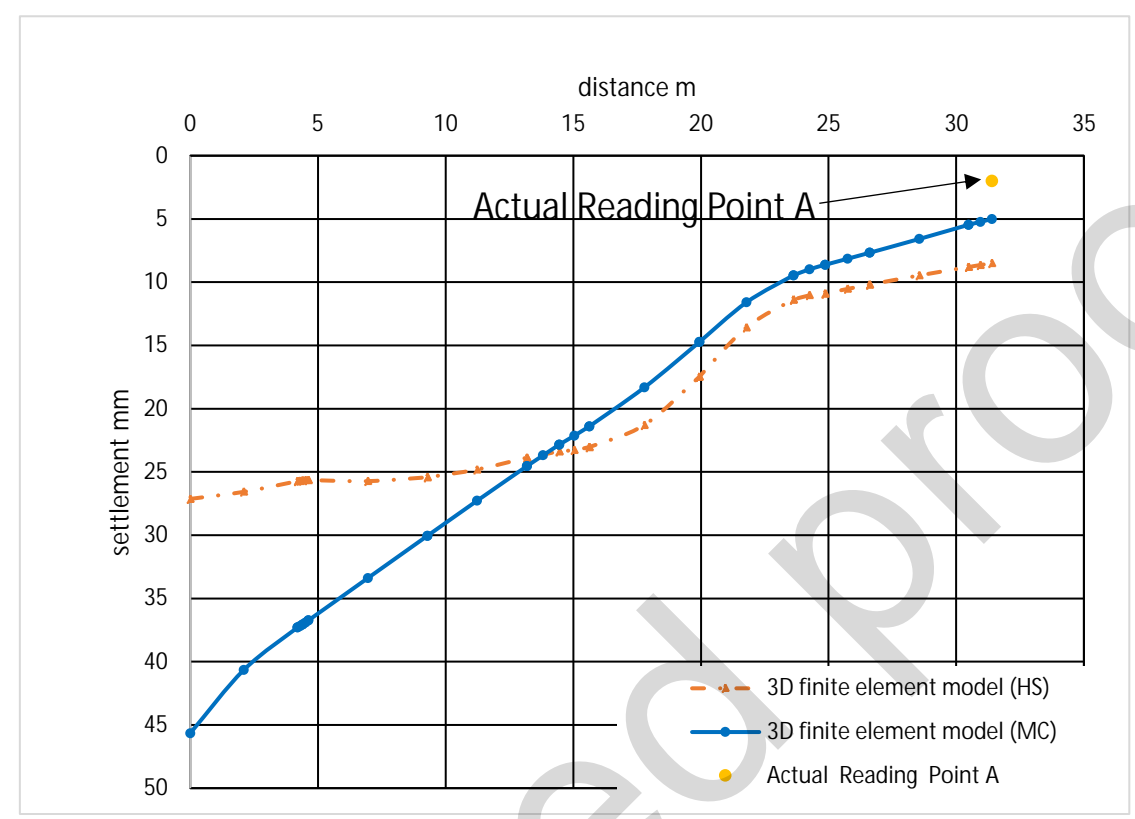


Fig. 18: 3D HS & MC The predicted settlement at the location of HEL25

Table 6: Comparison between Measured Settlement and Predicted Settlement from 3D Mohr-Coulomb (MC) and Hardening Soil (HS) Models

Surrounding Building	Max measured Settlement (mm)	Max predicted Settlement (mm)	measured / Predicted Settlement	% Max settlement / horizontal displaceme nt	% Max settlement / Depth of excavation
		3D-M	C		
HEL08 point(D)	3	21.73	0.138	19.828	0.105
HEL23	2	1.9	1.053	13.219	0.07
point(D)					
HEL25 point (A)	2	5	0.4	13.219	0.07
		3D-H	S		
HEL08	3	8.53	0.352	24.11	0.0299298
HEL23	2	6.07	0.329	16	0.0212983
HEL25	2	8.49	0.236	16	0.0297895

6. DISCUSSION

This section of the study looks at how well computer models can predict ground settlement caused by diaphragm wall construction. It starts by explaining why the study is important and compares the goals of 2D and 3D models. Then, it shows the results from both types of models and looks at how different they are. A PSR ratio is used to help compare the 2D and 3D results. The model predictions are checked against real field data to see how accurate they are. Finally, the performance of the models is reviewed to see how well they work.

6.1. Study Significance and Objective

This study addresses a critical gap in understanding the spatial behavior of diaphragm wall-supported deep excavations by performing a comparative analysis of two-dimensional (2D) and three-dimensional (3D) numerical simulations using Mohr–Coulomb (MC) and Hardening Soil (HS) models. While numerous studies have employed 2D modeling due to its simplicity and computational efficiency, fewer have quantified the variation introduced by transitioning to 3D, especially for complex urban excavations with significant structural interaction. By integrating real field data from multiple monitoring points in the Halophils Metro Station project, this study provides a reliable calibration benchmark for advanced numerical models. These insights are particularly valuable for geotechnical engineers, researchers, and designers seeking to optimize support systems while maintaining safety and serviceability standards in congested urban environments.

6.2. Comparison of 2D and 3D Numerical Results

Fig. 15 illustrates the differences in the deformed shapes produced by 2D and 3D numerical models. The results confirm that 3D simulations provide more realistic deformation patterns, especially in the vicinity of corners and complex structural boundaries. This is consistent with the findings of Hsiung et al. (2024), who demonstrated that 3D models are more accurately capture stress redistribution and deformation profiles in urban excavations [17]. **Fig. 16a** & **16b** show that, for both MC and HS models, the peak lateral deflection occurs near the mid-height of the diaphragm wall. Ou et al. (2006) observed similar trends in field-monitored wall systems, emphasizing the mid-depth as the most critical point for displacement [18]. In this study, the 2D MC model overestimated displacement by 11%, while the 3D MC model underestimated it by 8.74%, reinforcing the view of Bondareva et al. (2024) that 3D modeling provides improved accuracy in simulating excavation-induced deformations [19].

6.3. Plane Strain Ratio (PSR) Evaluation

The Plane Strain Ratio (PSR), which measures the ratio of maximum deflection from 3D to 2D simulations, offers a quantitative assessment of modeling dimensionality. This study reports a PSR of 0.956 for the MC model and 0.702 for the HS model, indicating significant sensitivity of the HS model to dimensional assumptions. As noted by Finno et al. (2006), PSR values substantially below unity suggest that 2D simulations may over-predict wall deformation unless calibrated [20].

6.4. Settlement Predictions and Model Validation

Figures 17 to **19** and **Table 6** present a detailed comparison of measured versus predicted settlements for points in buildings HEL8, HEL23, and HEL25. The 3D MC model consistently provided predictions closer to the field data, with a maximum deviation of 38%. Similar findings were reported by Lee et al. (2022), who highlighted the MC model's ability to approximate settlements in mixed soil conditions with reasonable accuracy [21]. Meanwhile, the 3D HS model produced more conservative estimates, underestimating settlements by up to 70%. This behavior aligns with the study by Hashash and Whittle (2002), who noted that the HS model, due to its nonlinear stress-dependent stiffness properties, often provides safer, though less accurate, settlement predictions [22].

6.5. Model Performance Assessment

In conclusion, while the 3D Mohr–Coulomb model offered superior accuracy in predicting ground deformation and settlement magnitudes, the 2D HS model aligned more closely with inclinometer

data for wall displacement. These findings validate the dual-approach methodology employing both 2D and 3D models for more comprehensive design and assessment of excavation systems, a strategy strongly recommended by previous scholars including Ou et al. (2006) and Finno et al. (2006) [18-20]. This study thus contributes meaningful benchmarks and evaluation metrics for modeling practices, particularly in metro construction and urban geotechnics, where empirical data are essential to validate simulation frameworks.

CONCLUSIONS

- 1. This study demonstrates that accurate numerical prediction of ground deformations associated with deep excavations is essential for the safe design and performance assessment of diaphragm walls, particularly in urban environments with closely spaced buildings and sensitive underground utilities. Using both the Mohr–Coulomb (MC) and Hardening Soil (HS) models implemented in PLAXIS, two-dimensional (2D) and three-dimensional (3D) simulations were conducted and benchmarked against field instrumentation data from the Halophils metro station project.
- 2. The analyses reveal that maximum lateral wall deformations consistently occur near the midheight of the diaphragm wall approximately 20 to 25 meters below ground level which corresponds well with inclinometer data. Among all models, the 3D Hardening Soil model produced the most accurate predictions, with deviations from field-measured lateral displacements limited to 8.74%. In contrast, the 2D Mohr–Coulomb model overestimated displacements by about 11%, highlighting the limitations of simplified plane strain assumptions in complex excavation scenarios.
- 3. Settlement analysis at three instrumented buildings (HEL8, HEL23, and HEL25) further supports the conclusion that 3D models, particularly those incorporating elasto-plastic hardening behavior, offer significantly improved agreement with observed data. While the 3D MC model captured general trends, it consistently overpredicted settlement magnitudes. Ground surface settlements were found to range between 6% and 32% of the corresponding maximum lateral wall displacements, indicating a substantial dependence on construction staging and soil-structure interaction.
- 4. The Plane Strain Ratio (PSR) values of 0.956 for the MC model and 0.702 for the HS model fall within the range reported by Lee et al. (1998) and other researchers, underscoring the importance of dimensional considerations in deformation prediction. These results reinforce the necessity of adopting 3D numerical approaches particularly with advanced constitutive models like Hardening Soil for reliable and performance-based design of retaining systems in geotechnical practice.
- 5. In conclusion, the study provides critical benchmarks for lateral deformation ratios and settlement- to-wall movement relationships that can guide future excavation designs. The findings also support the adoption of HS-based 3D modeling as a practical and validated tool for enhancing the predictive accuracy and safety of deep urban excavations.

CONFLICT OF INTEREST

The authors have no financial interest to declare in relation to the content of this article

REFERENCE

- [1] S. Suwansawat and H.H. Einstein, "Artificial neural networks for predicting the maximum surface settlement caused by EPB shield tunneling," Tunneling and Underground Space Technology, vol. 21, no. 2, pp. 133–150, 2006.
- [2] U.R. Zahid, H. Sajjad, T. Muhammad, M. Noor, S. Saira, and D. Nasrullah, "Prevention and mitigation management of tunnel collapse and failure during construction: A review," Int. J. Econ. Environ. Geol., vol. 12, no. 2, pp. 72–79, 2021.
- [3] R.B. Peck, "Deep excavation and tunneling in soft ground," Proceedings of the Seventh International Conference on Soil Mechanics and Foundation Engineering, Mexico City, Mexico, 1969, pp. 225–290.

- [4] P.G. Hsieh, T.C. Kung, C.Y. Ou, and Y.G. Tang, "Deep excavation analysis with consideration of small strain modulus and its degradation behavior of clay," Proceedings of the 12th Asian Regional Conference on Soil Mechanics and Geotechnical Engineering, Singapore, 2003.
- [5] M. Khoiri and C.Y. Ou, "Evaluation of deformation parameters for deep excavation in sand through case studies," Computers and Geotechnics, vol. 47, pp. 57–67, 2013.
- [6] E. Koh and T.S. Chua, "Multi earth retaining systems for an excavation project in Old Alluvium, Singapore," International Symposium on Advances in Foundation Engineering, Singapore, 2013.
- [7] P. Tedd, B.M. Chard, J.A. Charles, and I.F. Symons, "Behaviour of a propped embedded retaining wall in stiff clay at Bell Common Tunnel," Geotechnique, vol. 34, no. 4, pp. 513–532, 1984.
- [8] S.K.B. Siavash, G.N. Ashkan, and H. Alborz, "Study on horizontal displacement of restrained excavation walls by cantilever retaining wall," Int. J. Eng. Sci. Res. Technol., vol. 5, no. 6, pp. 847–852, 2016.
- [9] E.M. Comodromos, M.C. Papadopoulou, and G.K. Konstantinidis, "Effects on adjacent buildings from diaphragm wall installation," Proceedings of the 18th International Conference on Soil Mechanics and Geotechnical Engineering, Paris, France, 2013.
- [10] B.C.B. Hsiung and S.D. Dao, "Prediction of ground surface settlements caused by deep excavations in sands," Geotechnical Engineering Journal of the SEAGS & AGSSEA, vol. 46, no. 3, pp. 111–118, 2015.
- [11] K. Schanz, "The Hardening Soil Model," in Proceedings of the 1st International Conference on Computational Geotechnics, Oxford, 1998.
- [12] S. Suwansawat and H.H. Einstein, "Artificial neural networks for predicting the maximum surface settlement caused by EPB shield tunneling," Tunneling and Underground Space Technology, vol. 21, no. 2, pp. 133–150, 2006
- [13] C.F. Teo and K.S. Wong, "Simplified Estimation of Hardening Soil Parameters from SPT Data," in Proceedings of the 16th Southeast Asian Geotechnical Conference, Kuala Lumpur, Malaysia, 2007.
- [14] PLAXIS, Reference Manual, Plaxis BV, Delft, The Netherlands, 2016.
- [15] A.H. Abdel-Rahman and S.M. El-Sayed, "Foundation subsidence due to trenching of diaphragm walls and deep braced excavations in alluvium soils," in Proc. 17th Int. Conf. on Soil Mechanics and Geotechnical Engineering, Alexandria, Egypt, 2009.
- [16] M. Khoiri and C.Y. Ou, "Evaluation of deformation parameter for deep excavation in sand through case studies," Computers and Geotechnics, vol. 47, pp. 57–67, 2013.
- [17] Hsiung, B.C.B., Lee, C.C., & Chang, C.Y. (2024). Three-Dimensional Numerical Simulations of Corner Effects on Deep Excavations in Soft Ground. Buildings, 14(1), 23.
- [18] Ou, C.Y., Hsieh, P.G., & Chiou, D.C. (2006). Characteristics of ground surface settlement during excavation. Canadian Geotechnical Journal, 40(5), 1065–1077. https://doi.org/10.1139/t03-053
- [19] Bondareva, I., Grebneva, T., & Shved, M. (2024). Three-Dimensional Modeling of Deep Excavations with Diaphragm Walls. Bulletin of Civil Engineering, 1(32), 45–56. https://doi.org/10.32347/bf.knuba.2024.32.045
- [20] Finno, R.J., Lawrence, S.A., & Harahap, I.S. (2006). Performance of a Deep Excavation in Soft Clay. Journal of Geotechnical and Geoenvironmental Engineering, 132(4), 456–466. https://doi.org/10.1061/(ASCE)1090-0241(2006)132:4(456)
- [21] Lee, S.H., Ng, C.W.W., & Wang, L. (2022). Settlement Behavior of Structures Adjacent to Deep Excavations in Urban Areas. Soils and Foundations, 62(1), 221–233. https://doi.org/10.1016/j.sandf.2021.10.007
- [22] Hashash, Y.M.A., & Whittle, A.J. (2002). Ground movement prediction for deep excavations in soft clay. Journal of Geotechnical and Geoenvironmental Engineering, 128(6), 473–485. https://doi.org/10.1061/(ASCE)1090-0241(2002)128:6(473